SCIENCE CHINA
Physics, Mechanics & Astronomy

•Article•

February 2022 Vol. 65 No. 2: 229511
https://doi.org/10.1007/s11433-021-1818-1

Size, morphology, and composition of lunar samples returned by Chang'E-5 mission

Hui Zhang[1†], Xian Zhang[1†], Guang Zhang[1], Keqi Dong[1], Xiangjin Deng[2], Xiaosong Gao[3], Yaodong Yang[3], Yuan Xiao[1], Xiao Bai[1], Kaixin Liang[1], Yiwei Liu[1], Wenbin Ma[1], Shaofan Zhao[1], Ce Zhang[1], Xiaojing Zhang[1], Jian Song[1], Wei Yao[1], Hong Chen[4], Weihua Wang[1,5*], Zhigang Zou[1,6*], and Mengfei Yang[1,4*]

[1] *Qian Xuesen Laboratory of Space Technology, China Academy of Space Technology (CAST), Beijing 100094, China;*
[2] *Beijing Institute of Spacecraft System Engineering, China Academy of Space Technology (CAST), Beijing 100094, China;*
[3] *Materials and Processes Assurance Center of Beijing Spacecrafts, China Academy of Space Technology (CAST), Beijing 100094, China;*
[4] *China Academy of Space Technology (CAST), Beijing 100094, China;*
[5] *Institute of Physics, Chinese Academy of Sciences, Beijing 100190, China;*
[6] *College of Engineering and Applied Sciences, Nanjing University, Nanjing 210093, China*

Received November 4, 2021; accepted November 22, 2021; published online December 10, 2021

This study focuses on the physical and chemical properties of surficial lunar regolith (LR) samples returned from the Moon by the Chang'E-5 (CE-5) mission. Insights regarding the effect of a new sampling geological site on the surficial lunar sample CE5C0400 were illustrated using nondestructive techniques such as laser diffractometry coupled with image analysis, X-ray computed tomography, and field emission scanning electron microscopy equipped with energy dispersive spectroscopy, and X-ray diffraction combined with Rietveld refinement. From the characterization analyses, the CE-5 sampling site in the north-eastern Oceanus Procellarum on the Moon yields a unique collection of relatively regular-shaped and fine basalt-dominated particles. The median grain size D_{50} is (55.24±0.96) μm, falling within the relatively low end of the range of the Apollo lunar returned samples. The coefficient of uniformity C_u of 15.1 and the coefficient of curvature C_c of 1.7 could classify CE5C0400 to be well-graded. The minerals in CE5C0400 comprise approximately 44.5% pyroxene, 30.4% plagioclase, 3.6% olivine, and 6.0% ilmenite. There is a relatively low content of approximately 15.5% glass phase in the CE-5 lunar sample. From the results, we deduce that the CE-5 LR structure could have mainly resulted from micrometeoroid impacts to achieve such a high level of maturity.

the Moon, surface microscopy, meteoroid

PACS number(s): 96.20.-n, 68.37.-d, 96.30.Ys

Citation: H. Zhang, X. Zhang, G. Zhang, K. Dong, X. Deng, X. Gao, Y. Yang, Y. Xiao, X. Bai, K. Liang, Y. Liu, W. Ma, S. Zhao, C. Zhang, X. Zhang, J. Song, W. Yao, H. Chen, W. Wang, Z. Zou, and M. Yang, Size, morphology, and composition of lunar samples returned by Chang'E-5 mission, Sci. China-Phys. Mech. Astron. **65**, 229511 (2022), https://doi.org/10.1007/s11433-021-1818-1

*Corresponding authors (Mengfei Yang, email: yangmf@bice.org.cn; Zhigang Zou, email: zgzou@nju.edu.cn; Weihua Wang, email: whw@iphy.ac.cn)
†These authors contributed equally to this work.

1 Introduction

Lunar regolith (LR) [1], an interface with a typical thickness of several meters between the Moon and its space environment, contains essential information about the Moon source and future lunar resource utilization (LRU). Particularly, the surficial LR is of the most interest because various natural phenomena directly occur on it, including solar-wind injection, meteoritic/micrometeoritic impacts, cosmic ray bombardment, and space weathering [2-4]. The natural phenomena cause complex changes in the physical, chemical, and mineral characteristics associated with either outer atoms trapped in LR or physical melting and cementation of surface minerals [5]. Moreover, the LRU and lunar base establishment are mainly based on the detailed performance of LR [6]. Therefore, a clear understanding of the physical and chemical properties of LR is crucial for further lunar exploration.

To date, precious lunar samples returned from the US Apollo 11-17 missions and Soviet Luna programs have been extensively investigated for over 40 years [7,8]. A great deal of scientific data on the properties of the lunar returned samples, including mare volcanic and highland rocks, have comprehensively advanced the theories and knowledge of the Moon [9]. Nevertheless, the heterogeneous distribution of LR leads to a great variety of information depending on the sampling sites. Unexplored areas on the Moon are still broad [10]. New samples and novel analyses are considerably required to extend the data to wider regions of the Moon for better understanding [11].

Recently, the Chang'E-5 (CE-5) mission, the first mission to collect lunar samples in China, successfully brought back lunar samples. The CE-5 mission landed on a brand-new site (Figure 1), namely, a basaltic area in the northeastern Oceanus Procellarum in the northwest of the Moon [12]. The geological region is a broad lunar mare with dark gray plains in which volcanic activities last for a long time. Before launching, compared with the sampling sites of the US Apollo missions and Soviet luna programs (basalt ages of 3.1-3.9 billion years), the CE-5 sampling site was assessed to be unusually young (nearly 1.3-2 billion years) and to possess high scientific values by different researchers [13-16]. It is also confirmed from the latest studies [17-21] that such a unique sampling site for the CE-5 mission indeed yields brand-new lunar returned samples with unique properties.

Recently, our group has studied an invaluable surficial lunar sample (No. CE5C0400) returned from the CE-5 mission. Based on the unique sampling site, the top priority is to have a comprehensive understanding of the morphological, structural, chemical, and physical analyses on the surficial lunar sample CE5C0400. These properties are directly associated with the implantation of solar-wind elements, the addition of meteorite materials, and the grade and maturity of the lunar soil [22-24]. Besides, deeply understanding the LR properties would lay a solid foundation for future LRU activities on the Moon, such as mining and resource extraction [25]. Considering the historical importance of lunar samples, in this paper, we extensively investigate the physical and chemical properties of lunar samples using nondestructive techniques.

2 Material and method

2.1 Lunar samples

CAST photographs (Figure 1) presented the CE-5 LR with a dark gray appearance. The surficial samples of CE-5 LR were first extracted and investigated. The original lunar sample CE5C0400 derived from the precious surficial samples was stored in a glove box under clean and dry nitrogen gas before being explored. In the light of visual inspection, the lunar sample CE5C0400 looked dark gray and loosely stacked. In addition, it exhibited irregular sizes, with fine grains at the micron or submicron scale as well as large discernable particles at the submillimeter scale. A minimally necessary dose of the lunar sample CE5C0400 was used for each measurement described below due to inevitable exposure to the atmosphere when transferring from the glove box to test equipment.

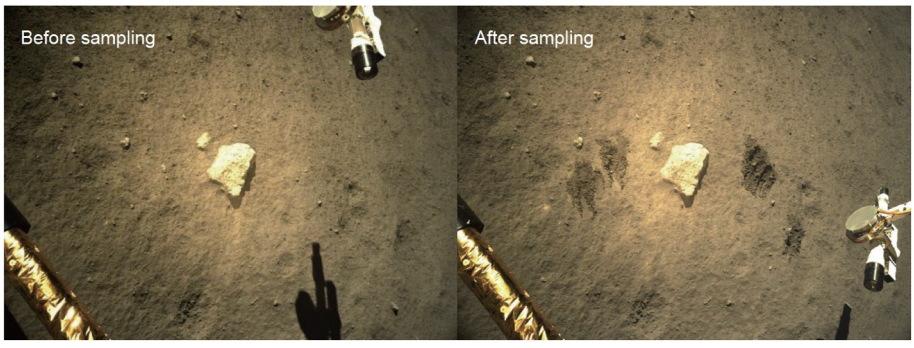

Figure 1 (Color online) On-site camera images of the sampling site of the Chang'E-5 mission before and after digging.

2.2 Optical and tomographic views

A collection of optical micrographs of the lunar sample CE5C0400 was obtained using a stereomicroscope (Nikon SMZ18). Prior to taking photographs, a small portion of the sample was placed in a laboratory glass dish, suspended in ethanol, and observed under the stereomicroscope when particles were dispersed. Meanwhile, the lunar sample CE5C0400 was observed by a V|tome|x S240 X-ray computed tomography (XCT) system (GE Sensing & Inspection Technologies GmbH), and their apparent shapes and interior structures were carefully investigated.

2.3 Particle size and shape distributions

Particle size and shape distributions for CE-5 LR were measured via a Bettersize 3000Plus laser diffractometer coupled with an image analyzer. The laser diffractometer with a light wavelength of 532 nm could analyze particle sizes between 0.01 and 3500 μm. While particle images were recorded and analyzed in the size range of 2-3500 μm.

2.4 Morphology and chemical composition

Field emission scanning electron microscopy (FESEM, Helios G4 CX, Thermofisher) equipped with an energy dispersive spectroscopy (EDS, X-MaxN 50, Oxford) detector was employed to investigate the morphology and chemical composition of the lunar sample CE5C0400. To protect the precious and historically significant lunar samples from contaminations, milligrams of the lunar sample CE5C0400 placed on carbon foil were not covered with any conductive materials. Such FESEM observations were performed at a low acceleration voltage of 2 kV to suppress the accumulation of electrostatic fields during imaging, and EDS surface scans were operated at an acceleration voltage of 18 kV under a high vacuum.

Powder X-ray diffractions (XRD) were collected on a Bruker D2 phaser diffractometer equipped with a monochromatized source of Cu Kα radiation (λ=0.15406 nm) at 4 kW (40 kV, 100 mA). Sample CE5C0400 was used without grinding, and the patterns were recorded in a slow-scanning mode with 2θ from 10° to 120° at a scan rate of 0.2°/min. Rietveld refinement was conducted to obtain the phase compositions for the lunar sample CE5C0400.

3 Results and discussion

Typical optical and XCT photographs of LR particles for sample CE5C0400 are shown in Figure 2. Figure 2(a) shows a cluster of agglutinates, glasses, and fragments of rocks and minerals, ranging from ~10 to ~200 μm. The particles possess various colors, including yellowish-green, off-white, brown, and dark gray, which are quite similar to the lunar sample returned by Apollo 11 [26]. Geologically, these colorful particles are believed to be olivine (yellowish-green), plagioclase (off-white), pyroxene or glass fragments (brown), and agglutinates (dark gray) [27]. Therefore, the crystalline minerals of the lunar sample CE5C0400 predominantly comprise pyroxene, plagioclase, and olivine. The particle shapes are highly variable, including the aciculiform, clavate, ellipsoidal, and spherical shapes, which can be observed in the reconstructed image from XCT measurements (Figure 2(f)). Several relatively large lithic fragments are found (Figure 2(c) and (d)) to be typical basalt fragments of lunar mare regions [28]. The representatively dark basalt fragment with a diameter of ~2 mm possesses an ophitic or subophitic-like texture (Figure 2(c)). Obviously, this basalt fragment comprises lath-shaped off-white plagioclase crystals surrounded by brown pyroxene and yellowish-green olivine. Some basalt particles also have a slightly glossier surface with signs of surface melting (Figure 2(d)).

An interesting feature observed in the lunar sample CE5C0400 is the occurrence of many agglutinates that are bonded with smaller particles (mineral grains, glasses, and even older agglutinates) together by vesicular, flow-banded glasses [29]. These agglutinates have irregular shapes and are typically mid-sized (100-200 μm) (Figure 2(b)). Most of their components have been melted and mixed into a dark glassy matrix, and there are pyroxene-based fragments that adhere to the outer surface. For example, a unique dumbbell-shaped agglutinate particle with mineral fragments adhering to its surface is depicted in Figure 2(e), which is very porous inside. The internal structure of an individual agglutinate particle was studied using XCT measurements (Figure 2(g)). The agglutinate particle is hollow, containing both closed and open voids. In addition, these internal voids in the particle have ellipsoidal and spherical shapes with sizes ranging from several to hundreds of micrometers. These features suggest that the voids are generated by the blister of components with relatively low boiling points [30,31].

Using an image analyzer combined with a laser diffractometer, the circularities of individual particles of the lunar sample CE5C0400 are analyzed based on two-dimensional images (Figure 3(a)) of 120597 particles between 15.0 and 438.2 μm. According to circularity distribution (Figure 3(b)), the average circularity is 0.875. More than 25% of the LR particles have circularity smaller than 0.854, and only 10% of those have circularity smaller than 0.805. As a result, most CE-5 LR particles possess high circularity and thus relatively regular shapes.

The particle size distribution of the lunar sample CE5C0400 derived from laser diffraction analysis is presented by both histograms of volume percent of particles and curve of cumulative volume distribution versus particle size

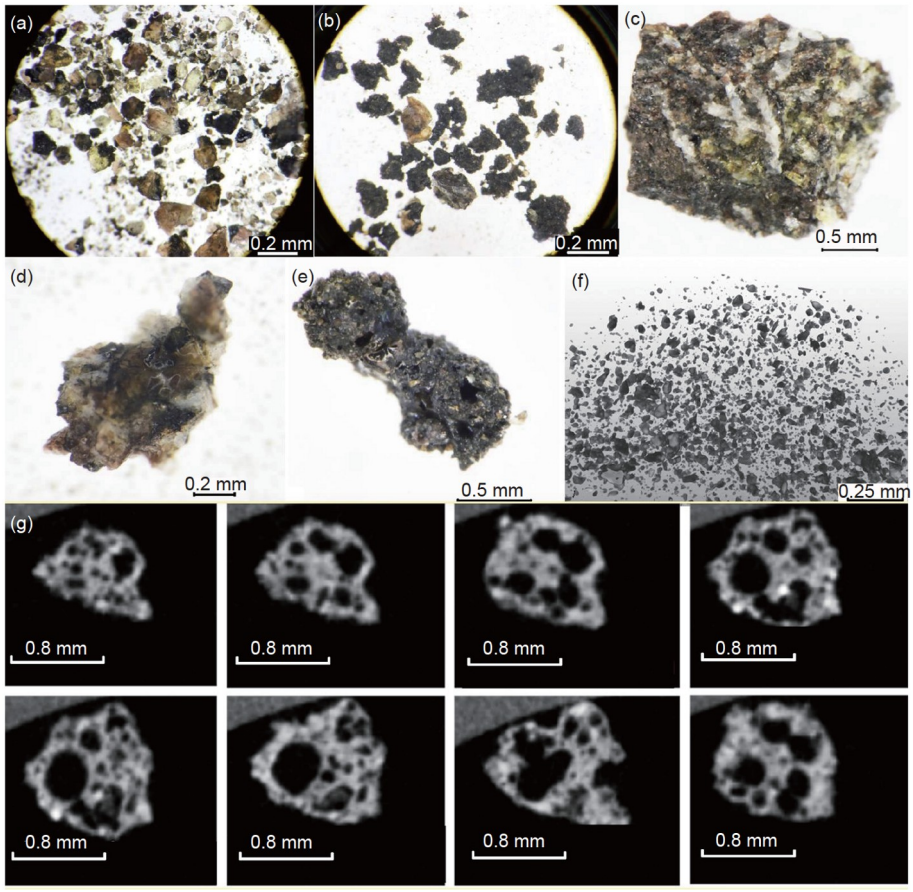

Figure 2 (Color online) Optical photographs of (a) multiple lunar regolith (LR) particles, (b) a group of agglutinates, (c) and (d) basalt-based fragments, and (e) a dumbbell-shaped agglutinate; (f) reconstructed image of LR particles and (g) X-ray computed tomography images of an agglutinate particle at various angles.

in Figure 3(c) and (d). In addition, Table 1 shows the relevant physical parameters for the lunar sample CE5C0400. As expected, a very broad distribution of particle size occurs in the range of 0.31-515.70 μm. There is a slow increment of volume percent in the size range of 1-10 μm, suggesting the existence of considerable quantities of fine dust. The volume percent gradually decreases when the particle size exceeds 86.35 μm, indicating a decrease in the number of large particles. The profile of the cumulative volume distribution (Figure 3(d)) yields the effective grain size D_{10}, middle grain size D_{30}, median grain size D_{50}, and constrained grain size D_{60} of (4.75±0.39), (24.34±0.91), (55.24±0.96), and (71.87±0.89) μm, respectively. In addition, Figure S1 shows the detailed tens of volume percent values corresponding to grain sizes with error bars from three running tests.

For most Apollo lunar samples, size distribution studies [32,33] were conducted by sieving the samples by weight. Recently, the median particle size of a CE-5 lunar sample (No. CE5C0800YJFM001) was reported to be 52.54 μm [19] according to size-mass distribution via image and statistical analyses. The difference from our results should be related to the size measurement method, in addition to the distinction of lunar samples. Using the same laser diffraction technique by size-volume distribution, the D_{50} value for the lunar sample CE5C0400 is in a median particle diameter range of 66.47-30.05 μm for Apollo 11 sample 10084 from a typical reference site: Mare Tranquillitatis [34]. Such a small D_{50} value implies a high level of maturity of CE-5 LR and a consequence of the monodisperse feature of the LR. The mature lunar soil has been also clarified by a recent report on CE-5 LR [19]. In addition, the coefficients of uniformity C_u and curvature C_c are 15.1 and 1.7, respectively. Thus, the lunar sample CE5C0400 can be described to be well-graded according to geotechnical criteria [35]. It is reasonable to deduce that the CE-5 LR structure could be mainly produced from micrometeoroid impacts to reach saturation closely.

Figure 4 depicts typical surface morphologies of CE5C0400 with various shapes and sizes. FESEM observations (Figure 4(a)) show that the LR particles are heterogeneous in appearance, including irregular, spherical, dendritic, angular, and block-like shapes. On average, more elongated and spherical particles in the size range of 10-100 μm are found, and the particles are largely derived from different minerals, agglutinates, debris fragments, and

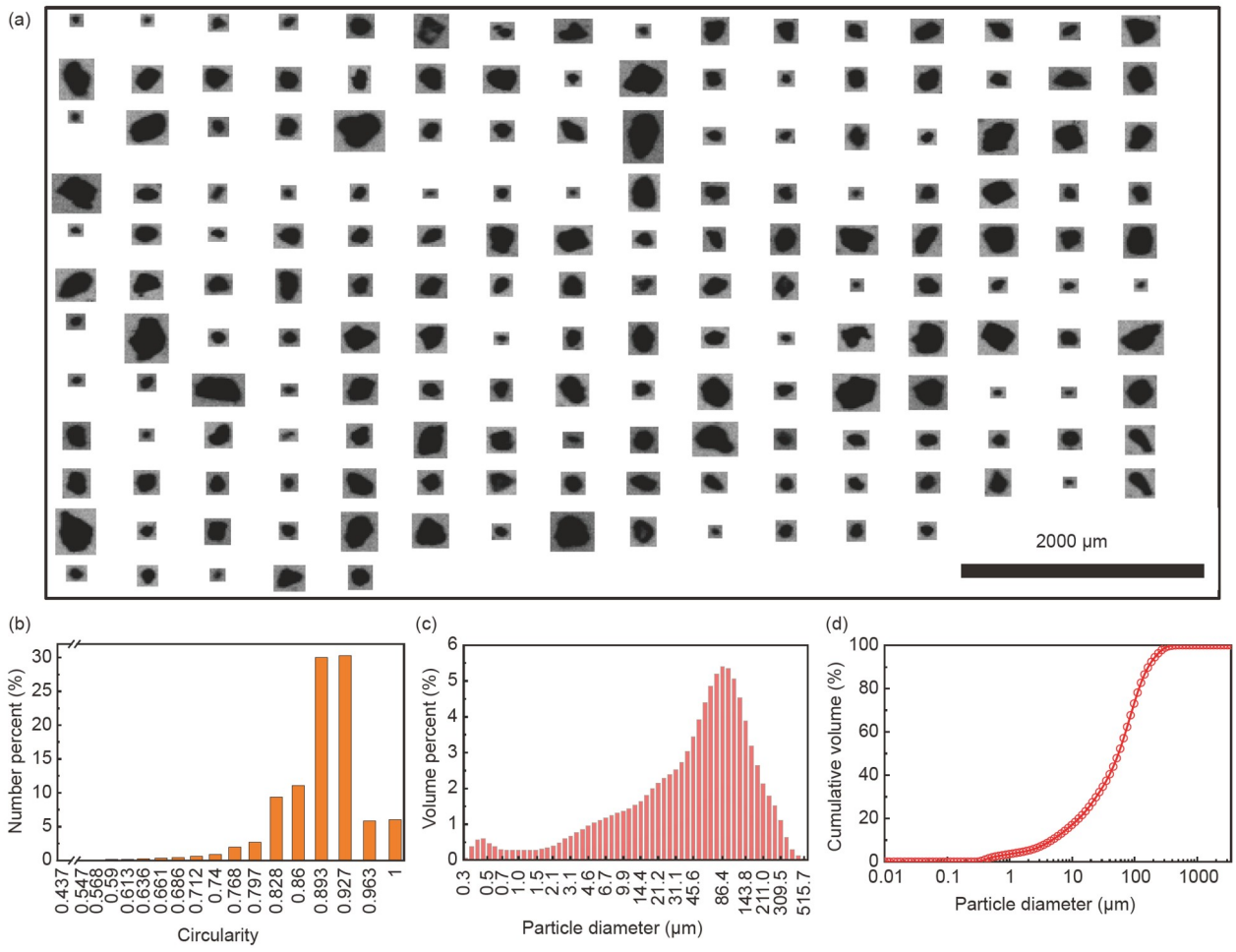

Figure 3 (Color online) Particle shape and size distributions of the lunar sample CE5C0400. (a) Representative images of individual particles via laser diffraction; (b) circularity distribution with sizes ranging from 15.0 to 438.2 μm; (c) volume percent distribution; (d) cumulative volume profile via laser diffraction.

Table 1 Basic physical properties of lunar sample CE5C0400 returned by the Chang'E-5 mission

Physical parameters	Value
Average circularity	0.875
Effective grain size, D_{10} (μm)	4.75±0.39
Middle grain size, D_{30} (μm)	24.34±0.91
Median grain size, D_{50} (μm)	55.24±0.96
Constrained grain size, D_{60} (μm)	71.87±0.89
Coefficient of uniformity, C_u	15.1
Coefficient of curvature, C_c	1.7

glass beads [28,36,37]. Two chosen crystal particles with clear rock textures of the lunar sample CE5C0400 are shown in Figure 4(b) and (c). Closeup views display that debris fragments and spherical droplets are distributed on the crystals. It is typical for LR samples to preserve some fragments from impact melts and older minerals because of micrometeoroid bombardment and volcanic eruption [1]. A relatively big agglutinate is clearly observed in Figure 4(d) in which small minerals and fragments with partially glassy surfaces are bonded together by a glassy matrix. Glass spherules containing native iron (Fe^0), as proven not to be uncommon [38], are also viewed on the agglutinate. A popular explanation [39] proposed that agglutinates formed by micrometeoroid impact implanted solar-wind elements, resulting in the partial reduction of iron oxide to iron (Fe^0). In addition, various circular and irregular vesicles with sizes ranging from 30 to 240 nm are observed on the surface of an agglutinate (Figure S2), which should be generated by the liberated solar-wind gases. Evidence for micrometeoroid impacts on the lunar surface is also provided by a bowl-shaped crater with a clear incision on an agglutinate and by an apparent fracture on a relatively large glass bead (~40 μm) in Figure 4(e) and (f). The Moon's population of impact craters represents an accurate record of these collisional processes over most of the solar system's lifetime [20,40].

FESEM observations combined with EDS surface scans are shown in Figures 4(g), (h), and S3 for composition

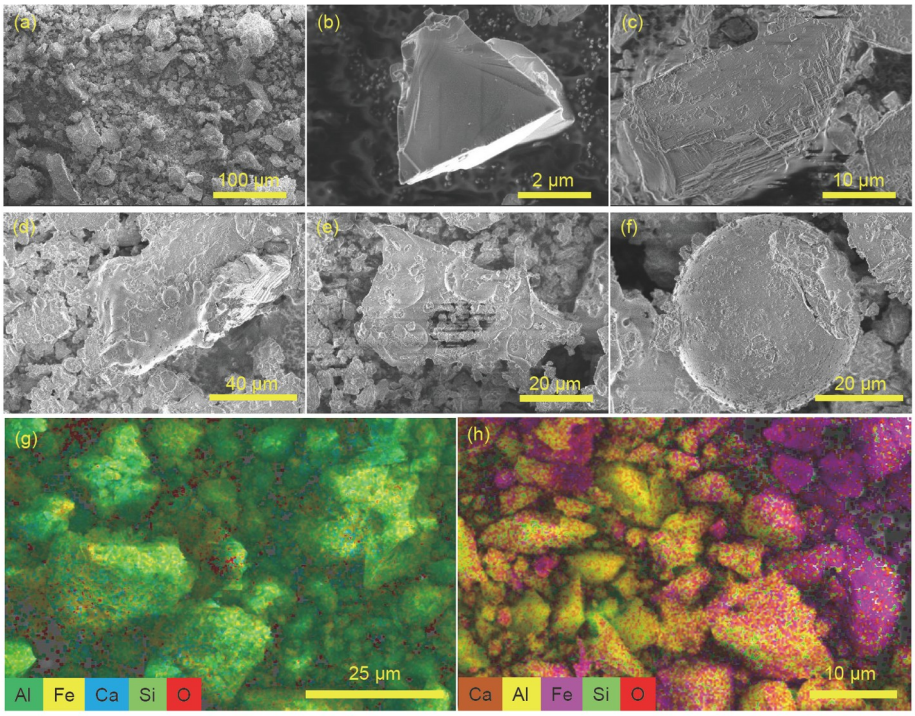

Figure 4 (Color online) FESEM images and EDS elemental distribution of the lunar sample CE5C0400. (a) Various irregular particles; (b) and (c) characteristic crystal particles; (d) a typical agglutinate with a partially glassy surface; (e) and (f) a crater on an agglutinate and fracture on a glass bead; (g) and (h) major element distribution using various colors in surface regions 1 (g) and 2 (h).

analysis of the lunar sample CE5C0400 in surface regions 1 and 2. The concentrations of the major elements are listed in Table 2. As expected [41,42], the lunar surfaces contain the two most abundant elements, i.e., approximately 60 at.% oxygen (O) and 15 at.% silicon (Si). For region 1, the other major elements are approximately 6.6 at.% aluminum (Al), 6.5 at.% Fe, 4.9 at.% calcium (Ca), 2.7 at.% magnesium (Mg), and 1.5 at.% titanium (Ti). The minor elements are sodium (Na), sulfur (S), potassium (K), chromium (Cr), and manganese (Mn). Highlights can be observed in the Fe element distribution, indicating Fe abundance in the lunar sample CE5C0400. The Fe-rich feature agrees with a recent report on CE-5 LR [19]. According to the ratios of the elements, it is reasonable to infer that the original mineral phases in the lunar sample CE5C0400 contain pyroxene ($(Ca,Mg,Fe)_2Si_2O_6$), olivine ($(Mg,Fe)_2SiO_4$), and plagioclase ($(Ca,Na)(Al,Si)_4O_8$).

In contrast, the elemental distribution in surface region 2 shows that Si, Al, Ca, and Mg concentrations are almost unchanged. Thus, there would be no obvious change in the amount of the plagioclase phase. Meanwhile, Fe and Ti concentrations increase to 9.0 at.% and 2.6 at.%, respectively, and O concentration decreases. The variations lead to the enlargement in the total valence ratio of cations:anions to be 123.3:118.2. The results manifest an increase in the concentration of pyroxene phase, and suggest the existence of Fe^0 and Fe,Ti-containing oxide minerals. Therefore, the surface domain is mainly composed of pyroxene, plagioclase, Fe^0, and Fe,Ti-containing oxide minerals. Similar to the Apollo lunar samples inside mare basalt regions [43], the elemental compositions of CE-5 lunar returned samples also depend on specific locations. From this work for sample CE5C0400, the young mare basalt at the CE-5 landing site could be deduced to be mostly dominated by pyroxene minerals.

The local surfaces of the lunar sample CE5C0400 with

Table 2 Representative surface composition of Chang'E-5 lunar regolith acquired from EDS surface scans in regions 1 and 2

Element	Region 1		Region 2	
	wt.%	at.%	wt.%	at.%
O	43.1	62.2	38.7	59.1
Na	0.5	0.5	–	–
Mg	2.9	2.7	2.7	2.8
Al	7.7	6.6	6.9	6.2
Si	18.0	14.8	17.2	15.0
S	0.2	0.1	–	–
K	0.2	0.1	0.2	0.1
Ca	8.5	4.9	8.2	5.0
Ti	3.0	1.5	5.1	2.6
Cr	0.2	0.1	0.4	0.2
Mn	0.2	0.1	–	–
Fe	15.6	6.5	20.6	9.0

small characteristic regions are further observed and analyzed in Figure S4; the corresponding elemental compositions are listed in Table S1. Angular ilmenite, Al-abundant plagioclase feldspar, and Ca-rich pyroxene particles are illustrated in Figure S4(a)-(c), respectively. The glass spherule (Figure S4(d)) with high Ca and Fe concentrations of up to 15.0 at.% and 35.4 at.%, respectively, could be apparently evolved from the original high-Ca pyroxene phase and Fe^0. The chemical analyses in the smooth and fragmentary areas on a big agglutinate reflect Mg-rich pyroxene and oxygen-enriched natures, respectively (Figure S4(e) and (f)). Further trace element analysis in high precision for the lunar sample CE5C0400 would be performed in future work.

To further confirm the major phases in the lunar sample CE5C0400, Figure 5 depicts the corresponding powder XRD profile. Combined with the results of major elements, the crystalline phases of the sample mainly comprise pyroxene (PDF#86-0005), plagioclase, olivine (PDF#99-0052), and ilmenite (PDF#99-0063). Besides, a broad peak appears from 20° to 35°, attributable to the presence of amorphous components. According to the Rietveld refinement in the inset of Figure 5, the main crystalline phases in the lunar sample CE5C0400 are approximately 44.5% pyroxene, 30.4% plagioclase, 3.6% olivine, and 6.0% ilmenite. The lunar sample CE5C0400 also contains approximately 15.5% amorphous phase.

4 Conclusion

The relationship between the CE-5 sampling site and performance of surficial LR (herein, CE5C0400) was primarily established, allowing the extension of LR data to broader geologic characterizations on the Moon. The CE-5 surficial lunar particles showed a high average circularity of 0.875 and a low median grain size of (55.24±0.96) μm, demonstrating a regular shape and very fine features. Meanwhile, basaltic minerals dominated by pyroxene, agglutinates containing minerals and glasses, glass beads containing native Fe, and diversified debris fragments were recognized with approximately 44.5% pyroxene, 30.4% plagioclase, 3.6% olivine, 6.0% ilmenite, and 15.5% glass. These provide evidence of the dominative consequence of micrometeoroid impacts on the lunar surface. Subsequent scientific interests include detailed interior structures and trace element analyses (e.g., rare earth and radioactive elements), the dynamic process of micrometeorite impacts, and the intrinsic properties of LRU.

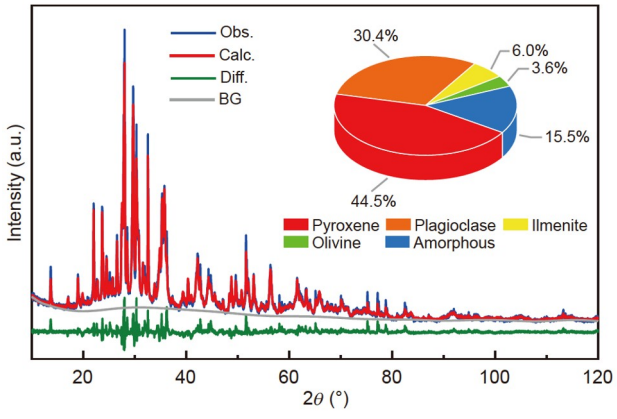

Figure 5 (Color online) Powder XRD pattern and the corresponding Rietveld refinement results for the lunar sample CE5C0400. The blue, red, green, and gray lines represent the observed value (Obs.), calculated value (Calc.), difference between the two values (Diff.), and background profiles (BG), respectively.

We would like to thank the China National Space Administration (CNSA) for providing us with the lunar sample.

Supporting Information

The supporting information is available online at http://phys.scichina.com and http://link.springer.com. The supporting materials are published as submitted, without typesetting or editing. The responsibility for scientific accuracy and content remains entirely with the authors.

1 D. S. McKay, G. Heiken, A. Basu, G. Blanford, S. Simon, R. Reedy, B. M. French, and J. Papike, *The Lunar Regolith: Lunar Sourcebook, A User's Guide to the Moon*, edited by G. H. Heiken, D. T. Vaniman, and B. M. French (Cambridge University Press, New York, 1991), pp. 285-356.
2 D. E. Gault, F. Hörz, and J. B. Hartung, Geochim. Cosmochim. Acta **3**, 2713 (1972).
3 C. E. Kenknight, D. L. Rosenberg, and G. K. Wehner, J. Geophys. Res. **72**, 3105 (1967).
4 E. A. King Jr., M. F. Carman, and J. C. Butler, Science **167**, 650 (1970).
5 E. A. King Jr., M. F. Carman, and J. C. Butler, Science **175**, 59 (1972).
6 D. G. Schrunk, B. L. Sharpe, B. L. Cooper, and M. Thangavelu, in *Lunar Origins and Physical Features: The Moon* (Praxis, Chichester UK, 2008), pp. 1-24.
7 J. J. Papike, S. B. Simon, and J. C. Laul, Rev. Geophys. **20**, 761 (1982).
8 G. Heiken, Rev. Geophys. **13**, 567 (1975).
9 E. Robens, A. Bischoff, A. Schreiber, A. Dąbrowski, and K. K. Unger, Appl. Surf. Sci. **253**, 5709 (2007).
10 Y. Langevin, and J. R. Arnold, Annu. Rev. Earth Planet. Sci. **5**, 449 (1977).
11 W. Yang, and Y. Lin, Innovation **2**, 100070 (2021).
12 Y. Qian, L. Xiao, J. W. Head, C. H. van der Bogert, H. Hiesinger, and L. Wilson, Earth Planet. Sci. Lett. **555**, 116702 (2021).
13 Y. Q. Qian, L. Xiao, S. Y. Zhao, J. N. Zhao, J. Huang, J. Flahaut, M. Martinot, J. W. Head, H. Hiesinger, and G. X. Wang, J. Geophys. Res. Planets **123**, 1407 (2018).
14 B. Wu, J. Huang, Y. Li, Y. Wang, and J. Peng, J. Geophys. Res. Planets **123**, 3256 (2018).
15 A. Neesemann, S. van Gasselt, N. Schmedemann, S. Marchi, S. H. G. Walter, F. Preusker, G. G. Michael, T. Kneissl, H. Hiesinger, R. Jaumann, T. Roatsch, C. A. Raymond, and C. T. Russell, Icarus **320**, 60 (2019).
16 M. N. Jia, Z. Y. Yue, K. C. Di, B. Liu, J. Z. Liu, and G. Michael, Earth Planet. Sci. Lett. **541**, 116272 (2020).
17 S. Hu, H. C. He, J. L. Ji, Y. T. Lin, H. J. Hui, M. Anand, R. Tartèse, Y. H. Yan, J. L. Hao, R. Y. Li, L. X. Gu, Q. Guo, H. Y. He, and Z. Y. Ouyang, Nature **600**, 49 (2021).

18 X. C. Che, A. Nemchin, D. Y. Liu, T. Long, C. Wang, M. D. Norman, K. H. Joy, R. Tartese, J. Head, B. Jolliff, J. F. Snape, C. R. Neal, M. J. Whitehouse, C. Crow, G. Benedix, F. Jourdan, Z. Q. Yang, C. Yang, J. H. Liu, S. W. Xie, Z. M. Bao, R. Fan, D. P. Li, Z. S. Li, and S. G. Webb, Science **374**, 887 (2021).

19 C. L. Li, H. Hu, M. F. Yang, Z. Y. Pei, Q. Zhou, X. Ren, B. Liu, D. Liu, X. G. Zeng, G. L. Zhang, H. B. Zhang, J. J. Liu, Q. Wang, X. J. Deng, C. J. Xiao, Y. G. Yao, D. S. Xue, W. Zuo, Y. Su, W. B. Wen, and Z. Y. Ouyang, Natl. Sci. Rev., doi: 10.1093/nsr/nwab188.

20 Q. L. Li, Q. Zhou, Y. Liu, Z. Y. Xiao, Y. T. Lin, J. H. Li, H. X. Ma, G. Q. Tang, S. Guo, X. Tang, J. Y. Yuan, J. Li, F. Y. Wu, Z. Y. Ouyang, C. Li, and X. H. Li, Nature **600**, 54 (2021).

21 H. C. Tian, H. Wang, Y. Chen, W. Yang, Q. Zhou, C. Zhang, H. L. Lin, C. Huang, S. T. Wu, L. H. Jia, L. Xu, D. Zhang, X. G. Li, R. Chang, Y. H. Yang, L. W. Xie, D. P. Zhang, G. L. Zhang, S. H. Yang, and F. Y. Wu, Nature **600**, 59 (2021).

22 E. N. Slyuta, Sol. Syst. Res. **48**, 330 (2014).

23 B. Hapke, W. Cassidy, and E. Wells, Science **264**, 1779 (1994).

24 J. A. Wood, J. Geophys. Res. **75**, 6497 (1970).

25 W. W. Mendell, *Lunar Bases and Space Activities of the 21st Century* (Lunar and Planetary Institute, Houston, 1985).

26 S. O. Agrell, J. H. Scoon, I. D. Muir, J. V. P. Long, J. D. C. McConnell, and A. Peckett, Science **167**, 583 (1970).

27 C. Kiely, G. Greenberg, and C. J. Kiely, Microsc. Microanal. **17**, 34 (2011).

28 Lunar Sample Preliminary Examination Team (1), Science **165**, 1211 (1969).

29 M. B. Duke, C. C. Woo, G. A. Sellers, M. L. Bird, and R. B. Finkelman, Geochim. Cosmochim. Acta **1**, 347 (1970).

30 T. Matsushima, J. Katagiri, K. Saiki, A. Tsuchiyama, M. Ohtake, T. Nakano, and K. Uesugi, in *3D Particle Characteristics of Highland Lunar Soil (No. 60501) Obtained by Micro X-Ray CT: Proceedings of the 11th Biennial Asce Aerospace Division International Conference on Engineering* (American Society of Civil Engineers, California, 2008), pp. 1-8.

31 S. Baidya, M. Melius, A. M. Hassan, A. Sharits, A. N. Chiaramonti, T. Lafarge, J. D. Goguen, and E. J. Garboczi, IEEE Geosci. Remote Sens. Lett., doi: 10.1109/LGRS.2021.3073344.

32 B. L. Cooper, K. Thaisen, B. C. Chang, T. S. Lee, and D. S. McKay, Nat. Geosci. **8**, 657 (2015).

33 W. D. Carrier, Moon **6**, 250 (1973).

34 B. L. Cooper, D. S. McKay, R. L. Fruland, and C. P. Gonzalez, in *Laser Diffraction Techniques Replace Sieving for Lunar Soil Particle Size Distribution Data: Proceedings of 43rd Lunar and Planetary Science Conference* (Lunar and Planetary Institute, The Woodlands, 2012), p. 2900.

35 B. W. Hapke, Planet. Space Sci. **16**, 101 (1968).

36 J. L. Carter, Geochim. Cosmochim. Acta **37**, 795 (1973).

37 Apollo 15 Preliminary Examination Team. Science **175**, 363 (1972).

38 S. Lim, J. Bowen, G. Degli-Alessandrini, M. Anand, A. Cowley, and V. Levin Prabhu, Sci. Rep. **11**, 2133 (2021).

39 E. Wells, and B. Hapke, Science **195**, 977 (1977).

40 M. R. Kirchoff, C. R. Chapman, S. Marchi, K. M. Curtis, B. Enke, and W. F. Bottke, Icarus **225**, 325 (2013).

41 W. D. Ehmann, and J. W. Morgan, Science **167**, 528 (1970).

42 G. H. Morrison, J. T. Gerard, A. T. Kashuba, E. V. Gangadharam, A. M. Rothenberg, N. M. Potter, and G. B. Miller, Science **167**, 505 (1970).

43 L. Haskin, and P. Warren, in *Lunar Chemistry*: *Lunar Sourcebook, A User's Guide to the Moon,*edited by G. H. Heiken, D. T. Vaniman, and B. M. French (Cambridge University Press, New York, 1991), pp. 357-474.